

RESEARCH ARTICLE

10.1029/2018JC014878

Key Points:

- Interannual variability of Antarctic Intermediate Water (AAIW) is found in the tropical North Atlantic
- Meridional propagating AAIW salinity anomalies are associated with the western boundary transport variability
- Zonal propagating AAIW anomalies may be related to baroclinic Rossby wave propagation

Supporting Information:

- Supporting Information S1

Correspondence to:

C. Wang,
 cwang@scsio.ac.cn

Citation:

Fu, Y., Wang, C., Brandt, P., & Greatbatch, R. J. (2019). Interannual variability of Antarctic Intermediate Water in the tropical North Atlantic. *Journal of Geophysical Research: Oceans*, 124, 4044–4057. <https://doi.org/10.1029/2018JC014878>

Received 18 DEC 2018

Accepted 17 MAY 2019

Accepted article online 22 MAY 2019

Published online 21 JUN 2019

Interannual Variability of Antarctic Intermediate Water in the Tropical North Atlantic

Yao Fu¹ , Chunzai Wang¹ , Peter Brandt^{2,3} , and Richard J. Greatbatch^{2,3} 

¹State Key Laboratory of Tropical Oceanography, South China Sea Institute of Oceanology, Chinese Academy of Sciences, Guangzhou, China, ²GEOMAR Helmholtz Centre for Ocean Research Kiel, Kiel, Germany, ³Faculty of Mathematics and Natural Sciences, Christian-Albrechts-Universität zu Kiel, Kiel, Germany

Abstract Interannual variability of Antarctic Intermediate Water (AAIW) in the tropical North Atlantic is investigated using the GECCO2 ocean state estimate and Argo data. AAIW salinity variability near the western boundary is highly correlated with the transport along the western boundary on interannual timescales. Northward propagating anomalies are associated with the western boundary transport variability that, to some extent, is related to the large-scale wind stress curl forcing by means of the Sverdrup balance. AAIW anomalies also propagate westward with the speed of baroclinic Rossby waves, indicating that the displacement of the meridional salinity gradient by westward propagation of baroclinic Rossby waves plays a role in the variability of AAIW characteristics. Slower eastward spreading of AAIW anomalies is identified on decadal timescales likely associated with the advection of salinity anomalies by weak eastward current bands. Understanding the observed interannual and decadal variability of AAIW salinity is important to properly interpret salinity changes reported in response to changes in the hydrological cycle.

Plain Language Summary Antarctic Intermediate Water (AAIW) is characterized by its low salinity in the ocean. Here we examine the variability of AAIW in the tropical North Atlantic on interannual timescales by using an ocean assimilation product (GECCO2) and Argo data. The analysis of these data shows that in the tropical northwestern Atlantic, variability of the AAIW salinity is associated with the transport variability near the western boundary and with the westward propagation of planetary waves. Decadal AAIW signals propagate eastward, which is indicative of eastward spreading of water mass anomalies with the weak circulation at intermediate depths. The identified AAIW water mass variability in the tropical North Atlantic has implications for the transport of tracers and particularly the ventilation of the oxygen minimum zone of the eastern tropical North Atlantic.

1. Introduction

Antarctic Intermediate Water (AAIW) is one of the major water masses of the World Ocean, originating from the Southern Hemisphere and participating in the global meridional overturning circulation (MOC). AAIW is formed just north of the Antarctic Circumpolar Current by subduction and spreads northward mainly along the western boundary (Tsuchiya, 1989). It is characterized by a salinity minimum associated with high oxygen and high nutrient levels lying between the subtropical thermocline and deep waters. The AAIW tongue of low salinity was first identified by the Meteor cruise during 1925–1927 (Wüst, 1935). In the Atlantic, as part of the upper limb of the Atlantic MOC (AMOC), AAIW plays an important role in the interhemispheric salinity, oxygen, and nutrient distribution (Palter & Lozier, 2008; Schmidtko & Johnson, 2012). Due to mixing with surrounding waters on its way northward, AAIW gradually loses the salinity minimum signature, which can be traced up to about 20°N (Tsuchiya, 1989). When AAIW reaches the tropical North Atlantic, its oxygen level has strongly reduced contributing to the lower part the oxygen minimum zone (OMZ) near the eastern boundary (e.g., Brandt et al., 2010, 2015; Stramma et al., 2008)

A number of studies have investigated the salinity and temperature changes in the intermediate layer of the Atlantic Ocean (Arbic & Owens, 2001; Fu et al., 2018; McCarthy et al., 2011; Sarafanov et al., 2007; Schmidtko & Johnson, 2012). Consistently, these studies revealed that during the last decades, AAIW became warmer and lighter in the South Atlantic, while it became warmer and more saline in the tropical North Atlantic. Causes for the AAIW property changes are still under investigation. A major contributor to the warming trend is thought to be the winter sea surface temperature increase in the AAIW formation region (Schmidtko & Johnson, 2012). An increased Agulhas leakage via changes in the southern annular

mode may also increase the AAIW salinity through enhanced export of salty Indian Ocean water to the Atlantic in the intermediate layer (Lübbecke et al., 2015). The increase in the Agulhas leakage during the last decades was suggested to be responsible for substantial salinity increase in the central water layer at the western boundary, with weaker but still significant salinity increase below in the intermediate water layer (Biaostoch et al., 2009; Durgadoo et al., 2013; Hummels et al., 2015). However, the salinification of AAIW in the tropical Atlantic does not seem to align with an enhanced hydrological cycle in the global warming scenario (e.g., Held & Soden, 2006). Fu et al. (2018) suggested that instead a weaker northward transport in the intermediate layer could be responsible for the observed AAIW salinification at 14.5°N in the Atlantic, highlighting the importance of water mass property changes along the spreading path due to entrainment and mixing with surrounding waters.

The tropical North Atlantic is the only ocean basin in the Northern Hemisphere, where a distinct AAIW salinity minimum can still be detected. Although long-term warming and salinification trends for AAIW in this region have been confirmed (Fu et al., 2018; Sarafanov et al., 2007; Schmidtko & Johnson, 2012), it remains unclear whether AAIW properties also vary on interannual timescales. In the South Atlantic, McCarthy et al. (2012) showed that the AAIW core salinity varies on interannual timescales with a peak to trough magnitude of 0.06. They attributed the variability to the westward propagation of planetary waves. In the tropical North Atlantic, a substantial influence from the more saline Mediterranean Water on AAIW can be anticipated. Near the eastern boundary, Machín and Pelegrí (2009) and Machín et al. (2010) showed a seasonally varying contribution of AAIW near the Canary Islands associated with shrinking and stretching of the intermediate water column. Near the western boundary, it has been shown by float observations and model studies that the North Brazil Current (NBC) and the associated NBC rings, formed after the NBC retroflects near French Guiana, play a dominant role in the northward transport of AAIW (Kirchner et al., 2009; Lankhorst et al., 2009). Additionally, AAIW is expected to ventilate the lower part of the thermocline in the tropics and subtropics. It also plays an important role in oxygen supply for the subtropical and tropical regions at lower thermocline and intermediate depths (Schmidtko & Johnson, 2012). A reduction of the ventilation in the depth range covered by AAIW could therefore contribute to the deoxygenation of the OMZ in the eastern tropical North Atlantic. Therefore, AAIW variability may have large dynamical and biological impact (Stramma et al., 2012).

In this study, we mainly use monthly data of the GECCO2 ocean state estimate (Köhl, 2015) and an Argo monthly climatology (Roemmich & Gilson, 2009) to investigate the variability of the AAIW core salinity in the tropical North Atlantic. We will focus on the western boundary region, since AAIW spreads northward mainly along the western boundary pathway, especially in the Northern Hemisphere (Figure 1). We show that on interannual timescales AAIW salinity variability is closely related to the variability of the transport near the western boundary and may also be associated with the westward propagation of long baroclinic Rossby waves.

2. Data and Climatology of the AAIW Core Salinity

2.1. Data

GECCO2 is an updated German version of the Massachusetts Institute of Technology general circulation model “Estimating the Circulation and Climate of the Ocean system (ECCO)” (Köhl & Stammer, 2008; Wunsch & Heimbach, 2006). It is a monthly mean product and has $1\times 1/3^\circ$ horizontal resolution, 50 vertical levels, and a time coverage from January 1949 to December 2014. At intermediate depths, the vertical resolution is approximately 90 m. This is sufficient for tracking the AAIW changes. GECCO2 applies the adjoint method to assimilate all available temperature and salinity profile data from the EN3 v2a database (Köhl, 2015); hence, it is expected to well represent the observed water mass properties. Note that for GECCO2, only data after 1985 are used, because it is expected that salinity observations at depth were rarely available before the late 1980s.

In order to verify the GECCO2 ocean state estimate, we use a monthly Argo product (Roemmich & Gilson, 2009) with 1° horizontal resolution, 58 vertical levels (for the upper 2000 m), and time coverage from 2004 to present. The vertical resolution of the Argo data at intermediate depth is 50 m. Note that in the first few years of the deployment, the number of Argo floats in the western tropical North Atlantic was relatively low and that the Argo floats are not evenly distributed throughout the whole period (Figure S1 in the

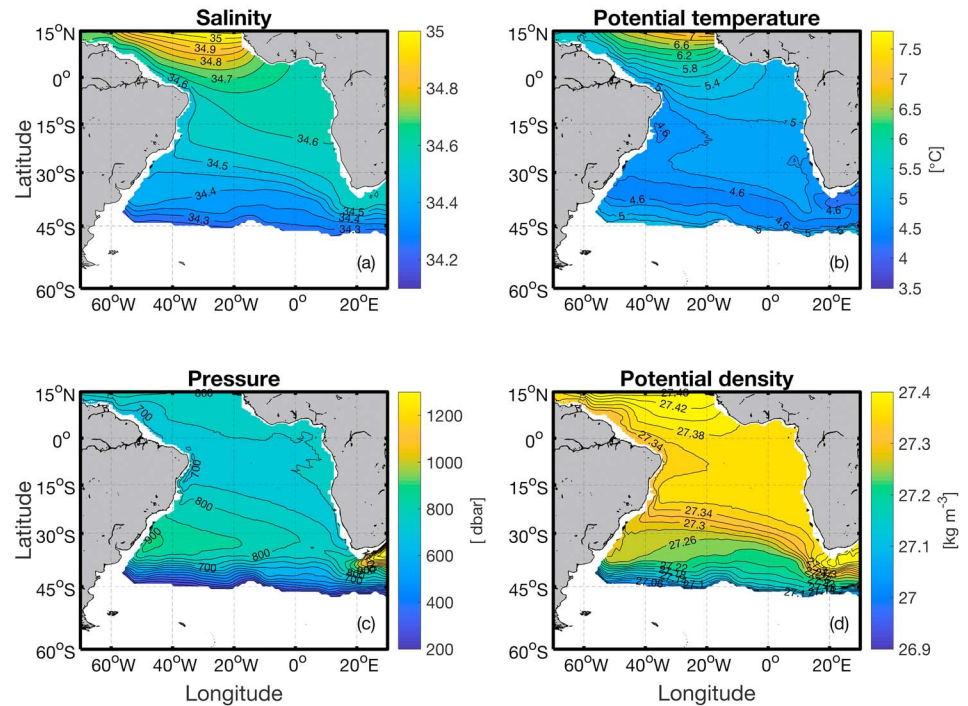


Figure 1. GECCO2 climatology (2004-2014) of the Antarctic Intermediate Water core properties in the Atlantic: (a) salinity, (b) potential temperature (referenced to the surface, in $^{\circ}\text{C}$), (c) pressure (in dbar), and (d) potential density (referenced to the surface, in kg/m^3).

supporting information). Fortunately, there are measurements covering AAIW depth near the western boundary within the longitude band of 60 to 55 $^{\circ}$ W in almost every year. However, one should still keep in mind that the uneven distribution of the Argo profiles may, to some extent, bias the results of this study.

To further verify the calculation results of GECCO2, we also use other ocean reanalysis products with monthly resolution, which include the Global Ocean Data Assimilation System (GODAS; Behringer & Xue, 2004), the ECMWF Ocean Reanalysis and derived ocean heat content (ORAS4, Balmaseda et al., 2013), Simple Ocean Data Assimilation (SODA) version 2.2.4 (Carton et al., 2008), and ECCO2 (Menemenlis et al., 2008). The horizontal resolution for GODAS is $1 \times \frac{1}{3}^{\circ}$ (longitude \times latitude), for ORAS4 $1 \times 1^{\circ}$, for SODA $0.5 \times 0.5^{\circ}$, and for ECCO2 $0.25 \times 0.25^{\circ}$. To keep consistency with GECCO2, the data after 1985 are used for each of the products. Finally, all data fields are vertically interpolated onto a uniform pressure grid of 10-dbar resolution using a spline interpolation method. All the calculations hereafter are based on the interpolated data. Note that the interpolation does not alter the calculation results significantly; it mainly improves the visual clarity for the anomalies shown below.

2.2. Overview of the AAIW Core Climatology

Following Schmidtko and Johnson (2012), we define the AAIW core for all data sets as the vertical salinity minimum within the neutral density range of 27.38 to 27.82 kg/m^3 from the monthly data. The salinity, potential temperature, pressure, and potential density at the depth of the AAIW core are used as the AAIW core properties. Potential temperature and potential density are referenced to the surface. Figures 1a to 1d show the GECCO2 climatological properties of the AAIW core in the Atlantic. For both GECCO2 and Argo, the climatological maps are generated using data between January 2004 and December 2014 to ease comparison. The core salinity gradually increases from north of the Antarctic Circumpolar Current to the subtropical North Atlantic, resulting from entrainment and mixing along its northward spreading path. In the Northern Hemisphere, low salinity is generally found along the western boundary, highlighting the western boundary pathway of AAIW. Although GECCO2 shows higher core salinity in comparison with Argo (Figure S2a), the overall basin-scale structure of salinity distribution in both products is consistent.

In GECCO2, the AAIW core potential temperature map (Figure 1b) shows a coherent structure similar to the salinity map, which is consistent with that of the Argo climatology in terms of magnitude and horizontal pattern (Figure S2b). The AAIW core is found primarily between 500 and 950 dbar in the Atlantic (Figures 1c and S2c). A difference in the core depth between GECCO2 and Argo is found in the tropical South Atlantic. The Argo core depth (Figure S2c) is relatively shallow (670 to 750 dbar) at the equator and southern latitudes of the tropics, while it is relatively deep (750 to 800 dbar) in between. This pattern is a result of the subtropical gyre circulation (Schmid et al., 2000; Schmid & Garzoli, 2009) but may not be adequately resolved by GECCO2 due to the coarse vertical resolution. Due to the higher salinity value in GECCO2, the AAIW core in GECCO2 is also denser than in Argo, but a northward increase of AAIW core potential density is still consistent with the northward salinity increase. In previous studies, GECCO2 is shown to well reproduce the observed ageostrophic flow and the AMOC in the tropical Atlantic (Fu et al., 2017, 2018). Therefore, a realistic representation of the strength of the western boundary current (WBC) system in the tropical North Atlantic is also expected. The overall agreement between the GECCO2 and Argo climatology of AAIW lends us confidence to use GECCO2 to analyze the dynamic variability of AAIW properties in the tropical North Atlantic.

3. Interannual Variability of AAIW

In order to investigate the interannual variability of AAIW, we first calculate the anomalies of the GECCO2 salinity and potential temperature at the AAIW core. The anomalies are calculated by subtracting the time-averaged salinity, potential temperature, and pressure at each grid point of GECCO2 between 2004 and 2014 from the monthly data. The monthly anomalies are then 3-year low-pass filtered. Analyzing the variability of AAIW at its core (salinity minimum) instead of on a certain density surface is preferable because salinity and potential temperature do not have to compensate each other at the salinity minimum and hence may vary differently.

3.1. Northward Propagating AAIW Core Anomalies

By using a Hovmoeller diagram of the low-pass filtered AAIW core salinity and potential temperature in the latitude and time directions, we first investigate the meridional propagation of AAIW (Figure 2). We chose a latitude band of 10 to 20°N along the 56°W meridian to generate the Hovmoeller diagram. This location is chosen to be close to the western boundary and to avoid the influence of the zonal equatorial current system. The Hovmoeller diagram shows a salinification trend of AAIW between 1985 and 2005, followed by a strong negative anomaly. The salinification of AAIW in the tropical North Atlantic in GECCO2 is consistent with the estimates based on hydrographic data (Fu et al., 2018; Schmidtko & Johnson, 2012), though the salinification trend in GECCO2 ($3 \times 10^{-3} \text{ year}^{-1}$) is somewhat stronger than the trend (about $1 \times 10^{-3} \text{ year}^{-1}$) estimated by Schmidtko and Johnson (2012). The stronger salinification trend in GECCO2 may result from the assimilation procedure, which alters the solution of the model toward all the available data. Northward propagating salinity anomalies are visible throughout most of the selected period. Similarities can also be detected in the potential temperature and pressure anomalies, though the warming trend and the meridional coherence in the potential temperature anomalies are not as obvious as in the salinity data. In the Argo data, northward propagating anomalies are also detectable (Figure S3). The phase of the anomaly propagation is consistent between Argo and GECCO2 data. A negative salinity anomaly also occurred after 2005 in the Argo data, but the magnitude of the anomaly is much smaller than in GECCO2. Note that the occurrence of the strong freshening in GECCO2 coincides with the availability of Argo data since 2004. Therefore, the stronger salinity variability in GECCO2 may be due to a superimposition of the dynamical variation of salinity and the model's adjustment toward lower salinity due to changes in the observational data (e.g., denser sampling by the Argo floats).

From the climatological map of the AAIW core salinity (Figure 1a), it can be anticipated that variability in the WBC system may play a dominant role in the northward export of fresh AAIW. To investigate the possible link between the WBC system and the northward propagating anomalies, we first define a WBC index. Since the coastline north of French Guiana is approximately zonal, here we select a meridional section from the coast to 10°N along 54°W. By assuming that the mean current here along the western boundary is predominantly zonal (Figure 3a), we then calculate the zonal transport across this section between 300 and 1,100 m (Figure 3b) as the WBC index. Note that the AAIW core is located at about 750 m in the studied

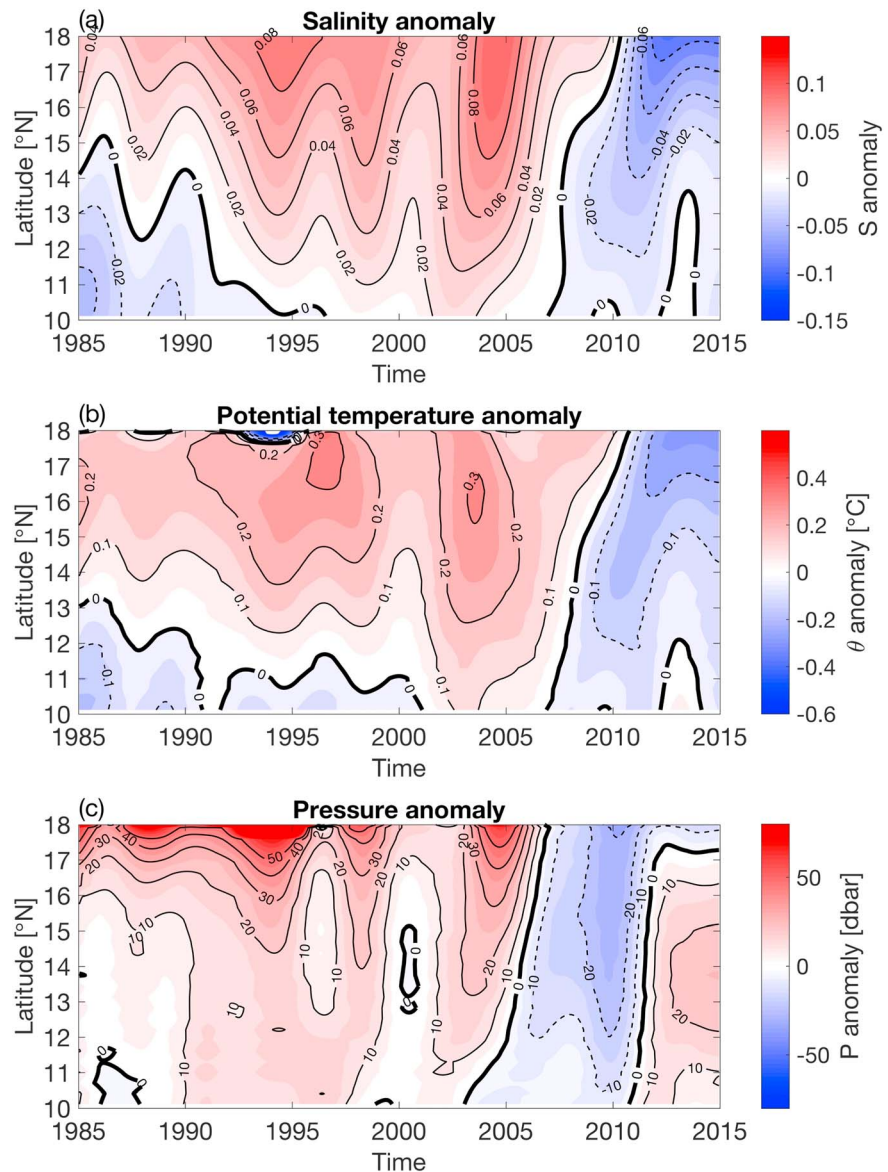


Figure 2. Latitude and time plot of the Antarctic Intermediate Water core anomalies of (a) Salinity, (b) potential temperature (in °C), and (c) pressure (in dbar) from GECCO2 along 56°W in the tropical North Atlantic.

area; therefore, we only consider this branch (300 to 1,100 m) of the transport along the western boundary when we investigate the relationship between the WBC system and the AAIW core salinity anomalies.

The Guiana Current represents a near-surface continuation of the NBC toward the Lesser Antilles after the main part of the NBC retroflects near French Guiana (Csanady, 1990). However, most of the northwestward transport is carried by the NBC rings migrating along the continental slope (e.g., Fratantoni et al., 2000; Fratantoni & Richardson, 2006; Johns et al., 1990, 2003). Detailed observations of the vertical structure of NBC rings revealed that these eddies partly have a deep structure reaching down to 1,000 m and more (Johns et al., 2003). The deep expression of the Guiana Current can be understood as the rectified mean flow associated with the migration of deep NBC rings. Depending on the horizontal resolution of the assimilation products, eddy activity may be represented differently in the different products. To examine the intensity of eddy activity in these products, we further calculated the eddy kinetic energy (EKE) and mean streamfunction at AAIW core depth using the flow field of each product (Figure S4). In general, eddy activity in the low-resolution products (GECCO2, GODAS, and ORAS4) is weakly resolved (i.e., lower EKE; Figures S4a, S4c, and S4e), while in the high-resolution products (SODA and ECCO2) they are clearly present (i.e., higher

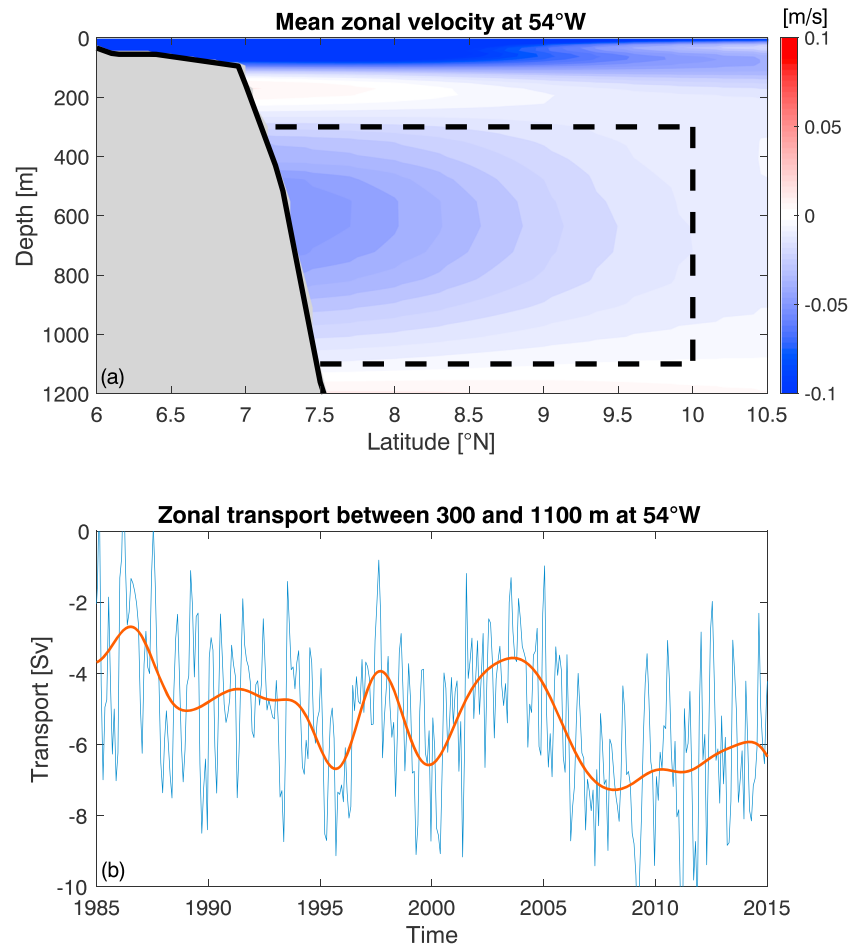


Figure 3. (a) Mean zonal velocity (in m/s) section at 54°W in the Atlantic, calculated from the GECCO2 data between 1985 and 2015. (b) The lower branch of the western boundary transport (in Sv) at 54°W, calculated as the zonal transport between 300 and 1,100 m, and between the coast and 10°N, as indicated by the black dashed box in (a). The blue thin curve is the monthly time series of the western boundary transport; the red curve is the 3-year low-pass filtered time series. Note that the transport is measured positive eastward.

EKE; Figures S4g and S4i). As a result, it seems that transport along the western boundary in the low-resolution products is probably done by a steady WBC (Figures S4b, S4d, and S4f), while in the high-resolution models it is mostly done by the eddies (e.g., NBC rings, Figures S4h and S4j). We will refer to the defined transport index as the western boundary transport rather than a specific current hereafter. The monthly salinity and western boundary transport anomalies are then 3-to-10-year band-pass filtered, so that only variability on interannual timescales is preserved. Note that the calculation results are not sensitive to the band-pass filtering window. Using a 2-to-10-year or 2-to-15-year filtering window does not alter the results shown later significantly.

The band-pass filtered GECCO2 western boundary transport is shown in Figure 4a. Also shown are the band-pass filtered GECCO2 salinity anomaly and the 3-year low-passed Argo salinity anomaly at 15°N, 56°W. Note that the Argo salinity time series is too short for a 3-to-10-year band-pass filter. The Argo salinity anomaly shows a peak to trough variation of about 0.04. This magnitude of salinity variation is consistent with a 0.06 AAIW salinity variation observed at 30°S in the Atlantic (McCarthy et al., 2012). It appears that on interannual timescales, the GECCO2 AAIW core salinity covaries with the western boundary transport at a lag of months to years. To illustrate how much the AAIW core salinity variability is related to the transport variability in GECCO2, we calculate a cross correlation between the western boundary transport and the AAIW core salinity at each grid point in the tropical northwestern Atlantic. The maximum correlation and the corresponding lag between the western boundary transport and the AAIW core salinity anomalies

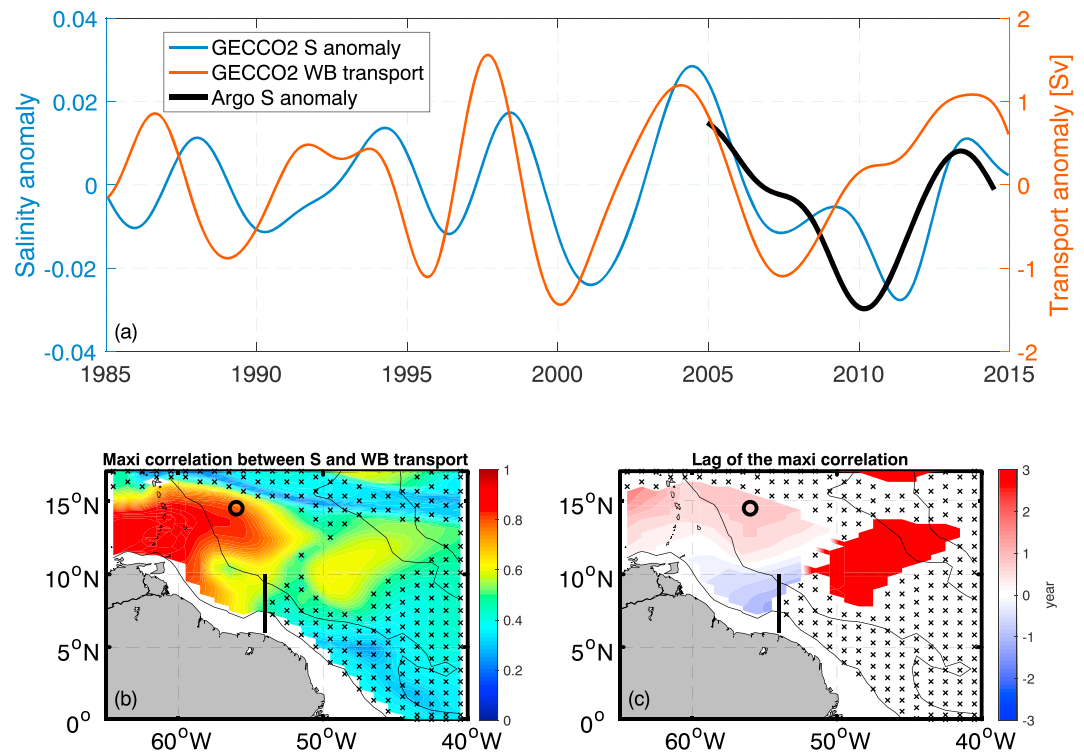


Figure 4. (a) The interannual variability of the GECCO2 Antarctic Intermediate Water (AAIW) core salinity at 14.5°N, 56°W (blue), GECCO2 western boundary transport (in Sv) between 300 and 1,200 m (red), and Argo AAIW core salinity at 14.5°N, 56°W (black). (b) The maximum cross-correlation between the western boundary transport and the AAIW core salinity in the tropical northwestern Atlantic. (c) The lead-lag relation between the western boundary transport and the AAIW core salinity at maximum correlation in (b). The black circles in (b) and (c) mark the position of 14.5°N, 56°W; the black meridional lines mark the position, where the western boundary transport is calculated. Note that both GECCO2 salinity and western boundary transport anomalies are band-pass filtered between 3 and 10 years, while the Argo salinity anomaly is only 3 years low-pass filtered. Correlations that are not significant on 95% confidence level are covered with crosses. The corresponding lags are also removed.

are shown in Figures 4b and 4c, respectively. The AAIW core salinity near the western boundary in the tropical North Atlantic is highly correlated to the western boundary transport with a correlation coefficient larger than 0.6. The corresponding lag for the maximum correlation increases northwestward (from negative to positive) with distance from the transport section along the western boundary. A positive (negative) lag indicates that the transport variability leads (lags) the salinity variability. Since transport is measured positive eastward and the transport across the selected section is mainly westward, a strengthening (weakening) of the transport corresponds to a negative (positive) anomaly. The high correlation in the western boundary regions suggests that a strengthening (weakening) of the western boundary transport is associated by a (an) decrease (increase) of the AAIW core salinity. Recall that the climatological AAIW core salinity increases from the south to the north (Figure 1a). The relationship between the western boundary transport and the AAIW core salinity can be explained by the fact that stronger (weaker) western boundary transport should export more (less) fresher AAIW from the South Atlantic to the tropical North Atlantic. This would decrease (increase) the observed salinity in the intermediate layer. The northwestward increasing lag with distance from the transport section also supports the observed northward propagation of the salinity anomaly in the GECCO2 and Argo data. In fact, the unfiltered western boundary transport time series (Figure 3b) shows an anomalous intensification between 2004 and 2008, which remains very strong till 2015. This corresponds to the strong freshening of the AAIW core since 2005 seen in Figure 2a. Note that there are also negative lags to the northwest of the transport section. This suggests that in the area of negative lags after minimum salinity is reached, a further strengthening of the western boundary transport leads to an increase of AAIW core salinity. To explain the negative lags, we calculate regressions of the western boundary

transport onto the velocity field and salinity at AAIW core depth with different lags in GECCO2 (Figure S5). In general, strengthening of the western boundary transport is associated with strengthening of northward velocity at AAIW core along the western boundary near French Guiana (i.e., when western boundary transport lags by 12 to 0 months). When the western boundary transport increases, salinity at the section starts to decrease. However, with increasing western boundary transport, a southeastward recirculation further offshore also develops and strengthens, which brings higher salinity water toward the coast from offshore. If the effect of recirculation on salinity dominates, it could lead to an increase of salinity already before the maximum western boundary transport is reached. This would complicate the relationship between the transport and salinity variability and could be responsible for the negative lags found in Figure 4c. In fact, the recirculation can also be seen in the mean streamline of GECCO2 (Figure S4b).

Additionally, we calculate the cross correlation between the AAIW core salinity and the western boundary transport using the other assimilation products. The derivation of the AAIW core salinity and the western boundary transport for these data sets is the same as for GECCO2. The maximum correlation and the corresponding lag for GODAS, ORAS4, SODA, and ECCO2 are shown in Figure 5. Among the products, GODAS, ORAS4, and ECCO2 show high correlation (>0.6) between the AAIW core salinity and the western boundary transport in the western boundary region (Figures 5a and 5c). The corresponding lags also increase northward with distance from the transport section (Figures 5b and 5d), indicative of northward propagation of the salinity anomalies. The negative lags in ORAS4 increase (approaching 0) continuously northward along the western boundary from about 5°N . This is also in agreement with the expectation that the salinity signals are transported by the WBC system from the south. To the northwest of the transport section, there are still negative lags, which could also be attributed to the recirculation in ORAS4 as can be seen in the mean streamline of ORAS4 at intermediate depth (Figure S4f). The results based on GODAS, ORAS4, and ECCO2 are consistent with that based on GECCO2, though the meridional extent of the high correlation in GODAS, ORAS4, and ECCO2 is not as far north as in GECCO2. For SODA-based calculation, although high correlation between the AAIW core salinity anomaly and the western boundary transport is visible, the lag for the maximum correlation does not reveal an alongshore structure like that seen in the other products (Figures 5e and 5f). A possible explanation would be that eddy activity is relatively strong in SODA, which may complicate the relationship between salinity variability and transport at the western boundary. However, as demonstrated by the results of ECCO2 with even higher resolution and stronger eddy activity, ECCO2 still shows high correlation and a northward increase of lags (Figures 5g and 5h). In fact, the SODA AAIW core salinity does not show any northward propagation signal as can be inferred from the Hovmoeller diagram (not shown). This is inconsistent with the Argo and other ocean reanalysis products, indicating that in the SODA assimilation, western boundary transport variability is unrelated to the AAIW salinity variability.

3.2. Zonal Propagating AAIW Core Anomalies

In the previous section, variability of the western boundary transport is proposed as a mechanism to explain the variability of the AAIW core salinity anomaly. In this section, we examine the zonal propagation of the AAIW core anomalies in GECCO2 by using a Hovmoeller diagram in longitude and time along 15°N (Figure 6). Apart from the salinification and warming trend, westward propagation stands out in both salinity and potential temperature anomalies on interannual timescales. The anomaly propagation can be analyzed using a two-dimensional Radon transform (Challenor et al., 2001; McCarthy et al., 2012), which returns information about the propagation speed of wavelike features. A dominant peak of the Radon transform corresponds to a westward propagation speed of 3.4 cm/s , as marked in Figure 6a. The application of the Radon transform at different latitudes shows that the anomaly propagation is generally faster at lower latitudes (about 4.2 cm/s at 10°N) and slower at higher latitudes (about 2.8 cm/s at 20°N). In the Argo data, westward anomaly propagation is most pronounced between 12 and 13°N with propagation speeds of 4.0 cm/s (not shown). The propagation speeds of the salinity anomaly in this latitude range are similar to the phase speed of the second-mode baroclinic Rossby waves in the same latitude range (Killworth & Blundell, 2003a, 2003b). McCarthy et al. (2012) also showed that along 30°S in the Atlantic, the AAIW salinity anomaly propagates westward in both Argo data and a high-resolution model simulation. Based on the overall consistency between the propagation speeds of salinity anomalies and second-mode baroclinic Rossby waves in that latitude band, McCarthy et al. (2012) attributed the westward anomaly propagation to the second

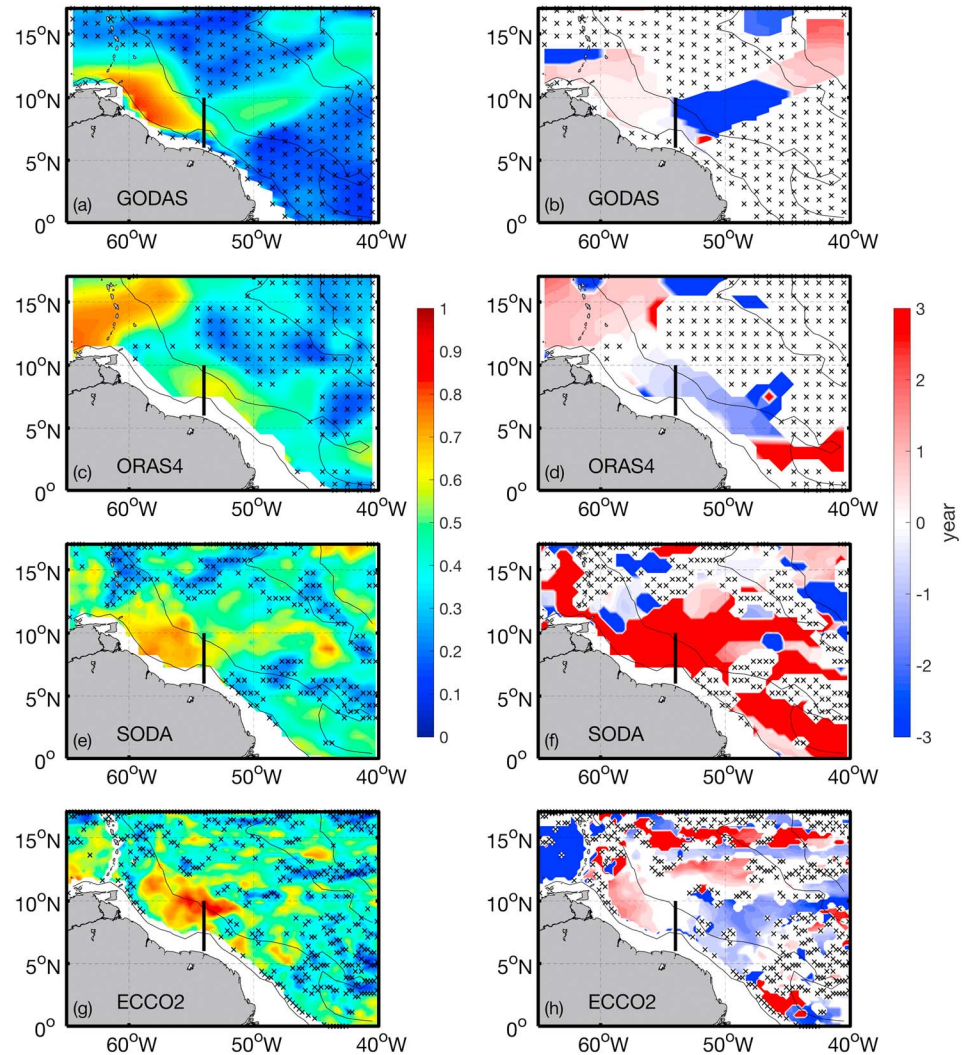


Figure 5. The maximum cross correlation and the lead-lag relation of the maximum correlation between the AAIW core salinity and the western boundary transport in the tropical northwestern Atlantic. The first panel (a and b) is calculated from the GODAS data, the second panel (c and d) from the ORAS4 data, the third panel (e and f) from the SODA data, and the last panel (g and h) from the ECCO2 data. Correlations that are not significant on 95% confidence level are covered with crosses. The corresponding lags are also removed. The position of the transport section is marked as the back thick line in each of the subplot. The western boundary transports in this plot are calculated in the same way as for GECCO2 (see Figure 4a and text for details). Positive lag indicates that the salinity variation lags the western boundary transport variation.

mode baroclinic Rossby waves. Our results based on the GECCO2 and Argo data also indicate that the zonal propagation of the salinity anomaly in the tropical North Atlantic may be related to the second-mode baroclinic Rossby waves. This may be explained by the westward propagation of the meridional velocity anomalies associated with the Rossby waves, which displace the latitudinal gradient of salinity at intermediate depth. As shown in Figure 1, the meridional gradients of salinity and temperature within the latitude band of 5°N to 15°N are relatively strong compared with the southern latitudes.

It is worth noting that the fast westward anomaly propagation is superimposed by a slow eastward spreading of salinity and temperature anomalies in GECCO2 on multidecadal timescales. This may be associated with the weak eastward current bands observed between 12 and 14°N (Brandt et al., 2015; Hahn et al., 2014), which could advect anomaly signals from the western boundary eastward and could eventually contribute to the observed changes in the OMZ in the eastern tropical North Atlantic (e.g., Hahn et al., 2017; Schmidtko & Johnson, 2012; Stramma et al., 2009). In fact, despite relatively low resolution, the mean

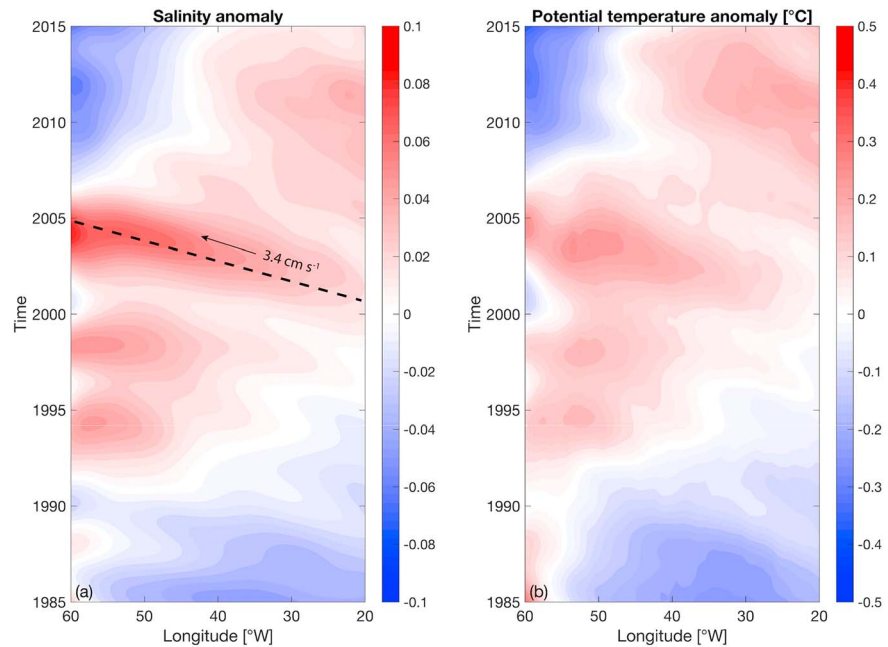


Figure 6. Longitude and time plot of the GECCO2 (a) salinity and (b) potential temperature (in °C) anomalies at Antarctic Intermediate Water core along 15°N in the Atlantic. On interannual timescales, westward propagation is clearly visible, while on decadal timescales, slow eastward spreading of salinity and temperature anomalies can also be detected.

meridional distribution of zonal velocity at 23°W in GECCO2 is quantitatively similar to the observations (e.g., Brandt et al., 2015; Hahn et al., 2014). For instance, weak eastward velocity in the lower thermocline and intermediate depth range can be detected in GECCO2 between 13 and 18°N. Additionally, Peña-Izquierdo et al. (2015) also showed that in ECCO2 the weak eastward velocity bands centered at 14°N extend down to 800 m. Peña-Izquierdo et al. (2015) referred to these velocity bands as the Cape Verde Current, which could account for the eastward transport of AAIW anomalies. However, it must be mentioned that among the other products, the slow eastward propagation of salinity and temperature anomalies on decadal timescales can only be seen in ECCO2 (not shown). Therefore, more caution may be needed when interpreting these long-term eastward progressing signals and longer record of observations is also required to verify these signals.

4. Summary and Discussion

In this study, the interannual variability of salinity and potential temperature at AAIW depth in the tropical North Atlantic has been investigated by using GECCO2, Argo, and other assimilation data. Northward and westward propagating salinity and potential temperature anomalies can be seen. Two major questions can be raised: what drives the propagating anomalies, and what is the implication of the observed AAIW variability?

By performing cross-correlation analysis using different assimilation products, we find that the AAIW salinity anomaly in the tropical North Atlantic is highly correlated with the lower branch (300–1,100 m) of the western boundary transport. Note that products with different resolutions present the transport near the western boundary in different forms. In the low-resolution models (GECCO2, GODAS, and ORAS4) the transport is mostly done by a steady WBC, while in the high-resolution models (SODA and ECCO2) it may be done by northwestward propagating eddies (i.e., NBC rings). However, both types of products generally show that the salinity anomaly variability lags the variability of the western boundary transport by months to years and the lag increases northwestward with distance from the transport section. This indicates that advection in the intermediate water layer by the transport along the western boundary plays a dominant role in the variability of AAIW salinity. As a salinity minimum, AAIW becomes more saline on the way of northward spreading, due to mixing with surrounding waters. A stronger (weaker) western boundary transport would carry more (less) fresher AAIW from the South Atlantic to the tropical North Atlantic, affecting the local salinity at intermediate depth. The northward propagation speed of salinity anomalies is also

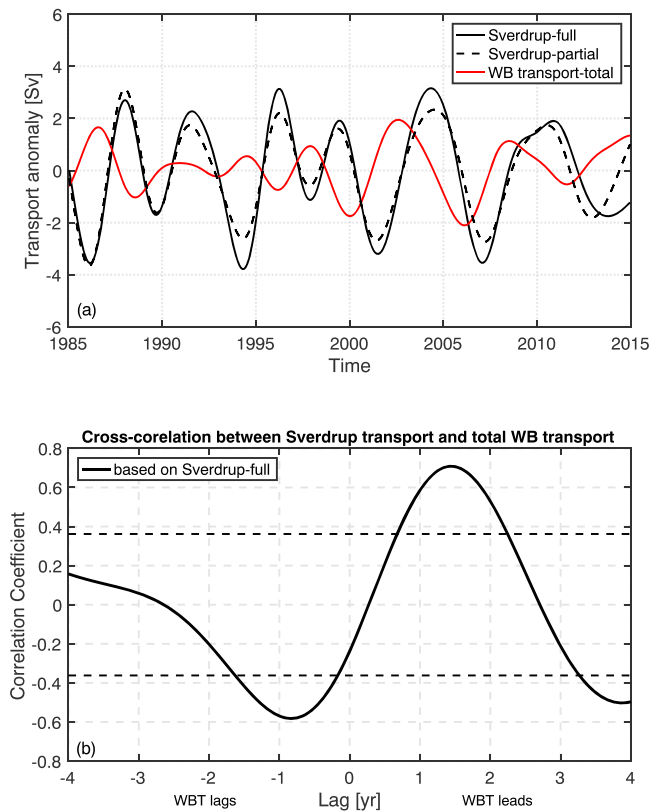


Figure 7. (a) Comparison between the Sverdrup transport (in Sv) time series at 8°N and the total western boundary transport (red, in Sv). The solid black curve is the Sverdrup transport calculated using full-basin-varying wind stress (Sverdrup-full), while the black dashed curve is the Sverdrup transport calculated by keeping the wind stress east of 30°W constant as the climatological mean and west of 30°W temporally varying (Sverdrup-partial). (b) Cross correlation between the Sverdrup-full and the total western boundary time series. Negative lag indicates that the Sverdrup transport leads, while positive lag indicates that the western boundary transport leads. All three time series in (a) are band pass filtered with cutoff frequency equivalent to 3 to 10 years. Correlations exceeding the black dashed lines are significant on 95% confidence level. The effective sample size for the significance test is determined following Bretherton et al. (1999). Note that the total western boundary transport is calculated the same as in Figure 3, except that the zonal velocity is integrated from the surface to 1,100 m. The mean flow across the transport section is westward, and transport is defined positive eastward. Therefore, a negative anomaly of the Sverdrup transport corresponds to a positive western boundary transport anomaly.

consistent with the advection due to the western boundary transport in GECCO2. For instance, between 2000 and 2006, the northward propagation speed, estimated using Radon transform, is about 1.0 cm/s. This is consistent with the long-term (1985-2014) areal mean velocity of the deep branch of the western boundary transport (1.3 cm/s westward) in GECCO2 (Figure 3). Note that anomaly propagation does not necessarily require variations in the circulation. A salinity anomaly may be carried northward by a steady current. However, in that case, one would not see a high correlation between the anomaly and transport, nor a gradually increasing lag with distance from the transport section.

To further examine the source of the western boundary transport variability, we computed the Sverdrup streamfunction from the monthly wind stress of GECCO2. A Sverdrup transport time series at 8°N is then extracted from the Sverdrup streamfunction (Text S1 in the supporting information). The sverdrup transport variability is significantly negatively correlated with the total western boundary transport variability, with the Sverdrup transport leading by about 10 months in GECCO2 (Figure 7). This is consistent with the expectation that a Sverdrup transport anomaly in the interior should induce a transport anomaly at the western boundary with reversed sign months to years later. The total western boundary transport is computed in the same way as the lower branch of the western boundary transport, except that the zonal velocity is integrated from the surface to 1,100 m. This indicates that on interannual timescales, variability of the western boundary transport results largely from the Sverdrup transport variability driven by large-scale wind stress curl in GECCO2. This result is consistent with the findings of Rühls et al. (2015), who showed that the interannual variability of the NBC at 6°S is mainly induced by the wind-driven gyre variability. Furthermore, in the calculation of the Sverdrup streamfunction, we test the sensitivity of the Sverdrup transport variability to the variability of the wind stress curl forcing at different longitudes. We found that if the wind stress curl east of 30°W is kept constant as the long-term mean value and west of 30°W is temporally varying, the resulting Sverdrup transport (black dashed line in Figure 7a) has similar magnitude and variability as the Sverdrup transport using full-basin-varying wind stress curl (black solid line in Figure 7a). This indicates that the wind-driven variability of the WBC mainly arises from the western two third of the basin. Note that a maximum correlation can also be found when the western boundary transport leads the Sverdrup transport by about 1.5 years, which is likely due to the autocorrelation of the two indices in GECCO2 introduced by the band-pass filtering of 3 to 10 years. It is worth noting that in the high-resolution ECCO2

product, significant negative correlation (-0.7) can also be found when the Sverdrup transport leads the western boundary transport by 7 months. However, the magnitude of the western boundary transport variability is much larger than that of the Sverdrup transport variability. This is an indication that in the high-resolution product, processes other than wind stress curl play a role in the western boundary transport variability. Given strong eddy activity in ECCO2, it can be anticipated that the presence of NBC rings may contribute largely to the variability of the western boundary transport. A period of 4 to 6 years can be detected in the Sverdrup transport time series in GECCO2, which is similar to the period of the Atlantic Meridional Mode (AMM). However, the Sverdrup transport time series is only marginally significantly correlated with the GECCO2 AMM index (defined following Foltz & McPhaden, 2010) with a 0.3 correlation coefficient (not shown). The sources of the 4-to-6-year variability of wind stress curl forcing are still not clear. It may result from a combined effect of different modes in the Atlantic (i.e., AMM, Atlantic Niño, and North Atlantic Oscillation) and need to be investigated further.

By applying a Radon transform, the zonal propagation speed of the AAIW anomalies is determined in GECCO2. Within the latitude range of 10 to 20°N, the zonal propagation speed of the anomalies varies between 2.8 and 4.2 cm/s and generally decreases with latitude in general agreement with latitude dispersion of Rossby waves. The anomaly propagation is consistent with the propagation speed of the second-mode baroclinic Rossby waves (Killworth & Blundell, 2003a, 2003b). This indicates that westward propagating Rossby waves may also play a role in the AAIW salinity variability, consistent with the findings in the South Atlantic by McCarthy et al. (2012). Baroclinic Rossby waves are generated through variations in wind stress curl forcing. They may induce anomalies in the meridional velocity field, which propagate westward associated with the Rossby waves. Therefore, instead of a zonal salinity transport, the westward propagation seen above might be due to a perturbation of the latitudinal gradient of salinity associated with the meridional velocity anomalies. In fact, wind-induced baroclinic Rossby waves are also known to remotely influence the WBC and the AMOC on interannual timescales (Clément et al., 2014; Zhao & Johns, 2014). Additionally, the latitude range of 10 to 20°N in the Atlantic covers part of the Cape Verde Frontal Zone (Zenk et al., 1991). It has been shown that baroclinic Rossby waves can also be excited through instability of the Cape Verde Frontal Zone (Spall, 1992).

As shown in Argo data, on interannual timescales, the AAIW salinity variability has a peak to trough magnitude of 0.04 in the tropical North Atlantic. This magnitude is comparable to that found in analyses of property changes at intermediate depth determined from repeated hydrographic surveys (Arbic & Owens, 2001; Curry et al., 2003; Fu et al., 2018). Traditional analysis of water masses based on hydrographic sections cannot account for the interannual variability of salinity, since the occupation of the sections is usually decades apart. Large salinity variability is expected to occur in the upper oceans due to eddy activity. However, at intermediate depth a 0.04 salinity variation may significantly bias the interpretation of salinity changes with respect to hydrological cycle. Therefore, any further study on AAIW salinity changes should not ignore such a variation.

In this study, we have demonstrated the connection between the AAIW property variability and the WBC on interannual timescales in the tropical North Atlantic. The WBC system, as a key component of the AMOC, exhibits also decadal to multidecadal variability (e.g., Rühls et al., 2015; Zhang et al., 2011). Rühls et al. (2015) demonstrated that on decadal to multidecadal timescales, NBC variations are forced by thermohaline forcing, which is superimposed by wind-driven gyre variability. As shown in Figure 6, apart from the westward propagating anomalies, a much slower eastward propagation of the anomalies on multidecadal timescales can be detected. This may be associated with the eastward advection of AAIW anomalies by the weak eastward current bands observed between 12 and 14°N (Brandt et al., 2015; Hahn et al., 2014; Peña-Izquierdo et al., 2015). In the Atlantic, long-term warming and salinification of AAIW have been shown in the observational data (Fu et al., 2018; Schmidtko & Johnson, 2012) and in GECCO2. These long-term water mass anomalies were attributed to changes in the atmospheric conditions in the AAIW formation region and an enhanced Agulhas leakage associated with variations in the southern annular mode (Lübbecke et al., 2015; Schmidtko & Johnson, 2012), and to a weaker transport in the intermediate layer, hence less fresher AAIW from the South Atlantic (Fu et al., 2018). As AAIW approaches the eastern boundary, it ventilates the lower part of the OMZ, therefore plays an important role in the oxygen supply to the OMZ in the eastern tropical North Atlantic. If the eastward spreading of the decadal salinity and potential temperature signals was associated with reduced ventilation in the AAIW layer, it could potentially contribute to a further deoxygenation of the OMZ. Therefore, AAIW variability and the corresponding mechanism on longer timescales (decadal to multidecadal) are relevant for biogeochemistry and ecosystem studies analyzing such long-term changes.

References

- Arbic, B. K., & Owens, W. B. (2001). Climatic warming of Atlantic intermediate waters. *Journal of Climate*, *14*(20), 4091–4108. [https://doi.org/10.1175/1520-0442\(2001\)014<4091:CWOAIW>2.0.CO;2](https://doi.org/10.1175/1520-0442(2001)014<4091:CWOAIW>2.0.CO;2)
- Balmaseda, M. A., Mogenssen, K., & Weaver, A. T. (2013). Evaluation of the ECMWF ocean reanalysis system ORAS4. *Quarterly Journal of the Royal Meteorological Society*, *139*(674), 1132–1161. <https://doi.org/10.1002/qj.2063>
- Behringer, D., & Xue, Y. (2004). Evaluation of the global ocean data assimilation system at NCEP: The Pacific Ocean. Eighth Symposium on Integrated Observing and Assimilation Systems for Atmosphere, Oceans, and Land Surface, AMS 84th Annual Meeting, Washington State Convention and Trade Center, Seattle, Washington, 11–15 January 2004.
- Biaostoch, A., Böning, C. W., Schwarzkopf, F. U., & Lutjeharms, J. R. E. (2009). Increase in Agulhas leakage due to poleward shift of Southern Hemisphere westerlies. *Nature*, *462*(7272), 495–498. <https://doi.org/10.1038/nature08519>

Acknowledgments

This study is supported by the National Natural Science Foundation of China (41731173), the Pioneer Hundred Talents Program of the Chinese Academy of Sciences, the Leading Talents of Guangdong Province Program, the Strategic Priority Research Program of the Chinese Academy of Sciences (XDA20060502), the National Program on Global Change and Air-Sea Interaction (GASI-IPOVAI-04), and by the Deutsche Forschungsgemeinschaft as part of cooperative project FOR1740. We appreciate the preliminary discussion with Sunke Schmidtko, which initiated this work and thank Ruixin Huang for helpful discussion. We also thank Jeff Blundell for providing the theoretical Rossby wave speed of Killworth and Blundell (2003a, 2003a, 2003b). The GECCO2, GODAS, ORAS4, SODA, and ECCO2 ocean reanalysis products are available at <http://icdc.cen.uni-hamburg.de/projekte/easy-init/easy-init-ocean.html>. The Argo data were collected and made freely available by the International Argo Program and the national programs that contribute to it (<http://www.argo.ucsd.edu>, <http://argo.jcommops.org>). The Argo Program is part of the Global Ocean Observing System (<https://doi.org/10.17882/42182>). This study was funded by the Deutsche Bundesministerium für Bildung und Forschung (BMBF) as part of the project RACE II (03F0651B).

- Brandt, P., Bange, H. W., Banyte, D., Dengler, M., Didwischus, S. H., Fischer, T., et al. (2015). On the role of circulation and mixing in the ventilation of oxygen minimum zones with a focus on the eastern tropical North Atlantic. *Biogeosciences*, *12*(2), 489–512. <https://doi.org/10.5194/bg-12-489-2015>
- Brandt, P., Hormann, V., Körtzinger, A., Visbeck, M., Krahmman, G., Stramma, L., et al. (2010). Changes in the ventilation of the oxygen minimum zone of the Tropical North Atlantic. *Journal of Physical Oceanography*, *40*(8), 1784–1801. <https://doi.org/10.1175/2010JPO4301.1>
- Bretherton, C. S., Widmann, M., Dymnikov, V. P., Wallace, J. M., & Bladé, I. (1999). The effective number of spatial degrees of freedom of a time-varying field. *Journal of Climate*, *12*(7), 1990–2009. [https://doi.org/10.1175/1520-0442\(1999\)012<1990:TENOSD>2.0.CO;2](https://doi.org/10.1175/1520-0442(1999)012<1990:TENOSD>2.0.CO;2)
- Carton, J. A., Giese, B. S., Carton, J. A., & Giese, B. S. (2008). A reanalysis of ocean climate using Simple Ocean Data Assimilation (SODA). *Monthly Weather Review*, *136*(8), 2999–3017. <https://doi.org/10.1175/2007MWR1978.1>
- Challenor, P. G., Cipollini, P., & Cromwell, D. (2001). Use of the 3D Radon transform to examine the properties of oceanic Rossby waves. *Journal of Atmospheric and Oceanic Technology*, *18*(9), 1558–1566. [https://doi.org/10.1175/1520-0426\(2001\)018<1558:UOTRTT>2.0.CO;2](https://doi.org/10.1175/1520-0426(2001)018<1558:UOTRTT>2.0.CO;2)
- Clément, L., Frajka-Williams, E., Szuts, Z. B., & Cunningham, S. A. (2014). Vertical structure of eddies and Rossby waves, and their effect on the Atlantic meridional overturning circulation at 26.5°N. *Journal of Geophysical Research: Oceans*, *119*, 6479–6498. <https://doi.org/10.1002/2014JC010146>
- Csanady, G. T. (1990). Retroflection and leakage in the North Brazil Current: Critical point analysis. *Journal of Marine Research*, *48*(4), 701–728. <https://doi.org/10.1357/002224090784988737>
- Curry, R., Dickson, B., & Yashayaev, I. (2003). A change in the freshwater balance of the Atlantic Ocean over the past four decades. *Nature*, *426*(6968), 826–829. <https://doi.org/10.1038/nature02206>
- Durgadoo, J. V., Loveday, B. R., Reason, C. J. C., Penven, P., & Biastoch, A. (2013). Agulhas Leakage predominantly responds to the Southern Hemisphere westerlies. *Journal of Physical Oceanography*, *43*(10), 2113–2131. <https://doi.org/10.1175/JPO-D-13-047.1>
- Foltz, G. R., & McPhaden, M. J. (2010). Interaction between the Atlantic meridional and Niño modes. *Geophysical Research Letters*, *37*, L18604. <https://doi.org/10.1029/2010GL044001>
- Fratantoni, D. M., Johns, W. E., Townsend, T. L., & Hurlburt, H. E. (2000). Low-latitude circulation and mass transport pathways in a model of the tropical Atlantic Ocean*. *Journal of Physical Oceanography*, *30*(8), 1944–1966. [https://doi.org/10.1175/1520-0485\(2000\)030<1944:LLCAMT>2.0.CO;2](https://doi.org/10.1175/1520-0485(2000)030<1944:LLCAMT>2.0.CO;2)
- Fratantoni, D. M., & Richardson, P. L. (2006). The evolution and demise of North Brazil current rings*. *Journal of Physical Oceanography*, *36*(7), 1241–1264. <https://doi.org/10.1175/JPO2907.1>
- Fu, Y., Karstensen, J., & Brandt, P. (2017). On the meridional ageostrophic transport in the tropical Atlantic. *Ocean Science*, *13*(4), 531–549. <https://doi.org/10.5194/os-13-531-2017>
- Fu, Y., Karstensen, J., & Brandt, P. (2018). Atlantic Meridional Overturning Circulation at 14.5° N in 1989 and 2013 and 24.5° N in 1992 and 2015: Volume, heat, and freshwater transports. *Ocean Science*, *14*(4), 589–616. <https://doi.org/10.5194/os-14-589-2018>
- Hahn, J., Brandt, P., Greatbatch, R. J., Krahmman, G., & Körtzinger, A. (2014). Oxygen variance and meridional oxygen supply in the Tropical North East Atlantic oxygen minimum zone. *Climate Dynamics*, *43*(11), 2999–3024. <https://doi.org/10.1007/s00382-014-2065-0>
- Hahn, J., Brandt, P., Schmidtko, S., & Krahmman, G. (2017). Decadal oxygen change in the eastern tropical North Atlantic. *Ocean Science*, *13*(4), 551–576. <https://doi.org/10.5194/os-13-551-2017>
- Held, I. M., & Soden, B. J. (2006). Robust responses of the hydrological cycle to global warming. *Journal of Climate*, *19*(21), 5686–5699. <https://doi.org/10.1175/JCLI3990.1>
- Hummels, R., Brandt, P., Dengler, M., Fischer, J., Araujo, M., Veleda, D., & Durgadoo, J. V. (2015). Interannual to decadal changes in the western boundary circulation in the Atlantic at 11°S. *Geophysical Research Letters*, *42*, 7615–7622. <https://doi.org/10.1002/2015GL065254>
- Johns, W. E., Lee, T. N., Schott, F. A., Zantopp, R. J., & Evans, R. H. (1990). The North Brazil Current retroflection: Seasonal structure and eddy variability. *Journal of Geophysical Research*, *95*(C12), 22103. <https://doi.org/10.1029/JC095iC12p22103>
- Johns, W. E., Zantopp, R. J., & Goni, G. J. (2003). Cross-gyre transport by North Brazil Current rings. *Elsevier Oceanography Series*, *68*, 411–441. [https://doi.org/10.1016/S0422-9894\(03\)80156-3](https://doi.org/10.1016/S0422-9894(03)80156-3)
- Killworth, P. D., & Blundell, J. R. (2003a). Long extratropical planetary wave propagation in the presence of slowly varying mean flow and bottom topography. Part II: Ray propagation and comparison with observations. *Journal of Physical Oceanography*, *33*(4), 802–821. [https://doi.org/10.1175/1520-0485\(2003\)33<802:LWPPI>2.0.CO;2](https://doi.org/10.1175/1520-0485(2003)33<802:LWPPI>2.0.CO;2)
- Killworth, P. D., & Blundell, J. R. (2003b). Long extratropical planetary wave propagation in the presence of slowly varying mean flow and bottom topography. Part I: The local problem. *Journal of Physical Oceanography*, *33*(4), 784–801. [https://doi.org/10.1175/1520-0485\(2003\)33<784:LWPPI>2.0.CO;2](https://doi.org/10.1175/1520-0485(2003)33<784:LWPPI>2.0.CO;2)
- Kirchner, K., Rhein, M., Hüttl-Kabus, S., & Böning, C. W. (2009). On the spreading of South Atlantic Water into the Northern Hemisphere. *Journal of Geophysical Research*, *114*, C05019. <https://doi.org/10.1029/2008JC005165>
- Köhl, A. (2015). Evaluation of the GECCO2 ocean synthesis: Transports of volume, heat and freshwater in the Atlantic. *Quarterly Journal of the Royal Meteorological Society*, *141*(686), 166–181. <https://doi.org/10.1002/qj.2347>
- Köhl, A., & Stammer, D. (2008). Variability of the meridional overturning in the North Atlantic from the 50-year GECCO state estimation. *Journal of Physical Oceanography*, *38*(9), 1913–1930. <https://doi.org/10.1175/2008JPO3775.1>
- Lankhorst, M., Fratantoni, D., Ollitrault, M., Richardson, P., Send, U., & Zenk, W. (2009). The mid-depth circulation of the northwestern tropical Atlantic observed by floats. *Deep-Sea Research Part I: Oceanographic Research Papers*, *56*(10), 1615–1632. <https://doi.org/10.1016/j.dsr.2009.06.002>
- Lübbecke, J. F., Durgadoo, J. V., & Biastoch, A. (2015). Contribution of increased agulhas leakage to tropical Atlantic warming. *Journal of Climate*, *28*(24), 9697–9706. <https://doi.org/10.1175/JCLI-D-15-0258.1>
- Machin, F., & Pelegrí, J. L. (2009). Northward penetration of Antarctic Intermediate Water off Northwest Africa. *Journal of Physical Oceanography*, *39*(3), 512–535. <https://doi.org/10.1175/2008JPO3825.1>
- Machin, F., Pelegrí, J. L., Fraile-Nuez, E., Vélez-Belchí, P., López-Laatzén, F., & Hernández-Guerra, A. (2010). Seasonal flow reversals of intermediate waters in the Canary Current System East of the Canary Islands. *Journal of Physical Oceanography*, *40*(8), 1902–1909. <https://doi.org/10.1175/2010JPO4320.1>
- McCarthy, G. D., King, B. A., Cipollini, P., McDonagh, E. L., Blundell, J. R., & Biastoch, A. (2012). On the sub-decadal variability of South Atlantic Antarctic Intermediate Water. *Geophysical Research Letters*, *39*, L10605. <https://doi.org/10.1029/2012GL051270>
- McCarthy, G. D., McDonagh, E., & King, B. (2011). Decadal variability of thermocline and intermediate waters at 24°S in the South Atlantic. *Journal of Physical Oceanography*, *41*(1), 157–165. <https://doi.org/10.1175/2010JPO4467.1>

- Menemenlis, D., Campin, J.-M., Heimbach, P., Hill, C. N., Lee, T., Nguyen, A. T., et al. (2008). ECCO2: High resolution global ocean and sea ice data synthesis. *Mercator Ocean Quarterly Newsletter*, 31, 13–21.
- Palter, J. B., & Lozier, M. S. (2008). On the source of Gulf Stream nutrients. *Journal of Geophysical Research*, 113, C06018. <https://doi.org/10.1029/2007JC004611>
- Peña-Izquierdo, J., van Sebille, E., Pelegrí, J. L., Sprintall, J., Mason, E., Llanillo, P. J., & Machín, F. (2015). Water mass pathways to the North Atlantic oxygen minimum zone. *Journal of Geophysical Research: Oceans*, 120, 3350–3372. <https://doi.org/10.1002/2014JC010557>
- Roemmich, D., & Gilson, J. (2009). The 2004–2008 mean and annual cycle of temperature, salinity, and steric height in the global ocean from the Argo Program. *Progress in Oceanography*, 82(2), 81–100. <https://doi.org/10.1016/j.pocean.2009.03.004>
- Rühs, S., Getzlaff, K., Durgadoo, J. V., Biastoch, A., & Böning, C. W. (2015). On the suitability of North Brazil Current transport estimates for monitoring basin-scale AMOC changes. *Geophysical Research Letters*, 42, 8072–8080. <https://doi.org/10.1002/2015GL065695>
- Sarafanov, A., Sokov, A., & Demidov, A. (2007). Water mass characteristics in the equatorial North Atlantic: A section nominally along 6.5°N, July 2000. *Journal of Geophysical Research*, 112, C12023. <https://doi.org/10.1029/2007JC004222>
- Schmid, C., & Garzoli, S. L. (2009). New observations of the spreading and variability of the Antarctic Intermediate Water in the Atlantic. *Journal of Marine Research*, 67(6), 815–843. <https://doi.org/10.1357/002224009792006151>
- Schmid, C., Siedler, G., & Zenk, W. (2000). Dynamics of intermediate water circulation in the subtropical South Atlantic*. *Journal of Physical Oceanography*, 30(12), 3191–3211. [https://doi.org/10.1175/1520-0485\(2000\)030<3191:DOIWCI>2.0.CO;2](https://doi.org/10.1175/1520-0485(2000)030<3191:DOIWCI>2.0.CO;2)
- Schmidtko, S., & Johnson, G. C. (2012). Multidecadal warming and shoaling of Antarctic Intermediate Water. *Journal of Climate*, 25(1), 207–221. <https://doi.org/10.1175/JCLI-D-11-00021.1>
- Spall, M. A. (1992). Rossby wave radiation in the Cape Verde Frontal Zone. *Journal of Physical Oceanography*, 22(7), 796–807. [https://doi.org/10.1175/1520-0485\(1992\)022<0796:RWRITC>2.0.CO;2](https://doi.org/10.1175/1520-0485(1992)022<0796:RWRITC>2.0.CO;2)
- Stramma, L., Johnson, G. C., Sprintall, J., & Mohrholz, V. (2008). Expanding oxygen-minimum zones in the tropical oceans. *Science*, 320(5876), 655–658. <https://doi.org/10.1126/science.1153847>
- Stramma, L., Oschlies, A., & Schmidtko, S. (2012). Mismatch between observed and modeled trends in dissolved upper-ocean oxygen over the last 50 yr. *Biogeosciences*, 9(10), 4045–4057. <https://doi.org/10.5194/bg-9-4045-2012>
- Stramma, L., Visbeck, M., Brandt, P., Tanhua, T., & Wallace, D. (2009). Deoxygenation in the oxygen minimum zone of the eastern tropical North Atlantic. *Geophysical Research Letters*, 36, L20607. <https://doi.org/10.1029/2009GL039593>
- Tsuchiya, M. (1989). Circulation of the Antarctic Intermediate Water in the North Atlantic Ocean. *Journal of Marine Research*, 47(4), 747–755. <https://doi.org/10.1357/002224089785076136>
- Wunsch, C. I., & Heimbach, P. (2006). Estimated decadal changes in the North Atlantic Meridional overturning circulation and heat flux 1993–2004. *Journal of Physical Oceanography*, 36(11), 2012–2024. <https://doi.org/10.1175/JPO2957.1>
- Wüst, G. (1935). Schichtung und Zirkulation des Atlantischen Ozeans, Die Stratophäre. In *Wissenschaftliche Ergebnisse der Deutschen Atlantischen Expedition auf dem Forschungs- und Vermessungsschiff "Meteor" 1925–1927*, (Chap. 2, Vol. 6, pp. 109–288). Berlin: Walter de Gruyter.
- Zenk, W., Klein, B., & Schroder, M. (1991). Cape Verde Frontal Zone. *Deep Sea Research Part A. Oceanographic Research Papers*, 38, S505–S530. [https://doi.org/10.1016/S0198-0149\(12\)80022-7](https://doi.org/10.1016/S0198-0149(12)80022-7)
- Zhang, D., Msadek, R., McPhaden, M. J., & Delworth, T. (2011). Multidecadal variability of the North Brazil Current and its connection to the Atlantic meridional overturning circulation. *Journal of Geophysical Research*, 116, C04012. <https://doi.org/10.1029/2010JC006812>
- Zhao, J., & Johns, W. (2014). Wind-forced interannual variability of the Atlantic Meridional Overturning Circulation at 26.5°N. *Journal of Geophysical Research: Oceans*, 119, 2403–2419. <https://doi.org/10.1002/2013JC009407>